Effects of flow on the dynamics of a ferromagnetic nematic liquid crystal

Tilen Potisk,[1,2,*] Harald Pleiner,[3] Daniel Svenšek,[2] and Helmut R. Brand[1]

[1]*Department of Physics, University of Bayreuth, 95440 Bayreuth, Germany*
[2]*Department of Physics, Faculty of Mathematics and Physics, University of Ljubljana, SI-1000 Ljubljana, Slovenia*
[3]*Max Planck Institute for Polymer Research, 55021 Mainz, Germany*

We investigate the effects of flow on the dynamics of ferromagnetic nematic liquid crystals. As a model, we study the coupled dynamics of the magnetization, $\mathbf{M}$, the director field, $\mathbf{n}$, associated with the liquid crystalline orientational order, and the velocity field, $\mathbf{v}$. We evaluate how simple shear flow in a ferromagnetic nematic is modified in the presence of small external magnetic fields, and we make experimentally testable predictions for the resulting effective shear viscosity: an increase by a factor of 2 in a magnetic field of about 20 mT. Flow alignment, a characteristic feature of classical uniaxial nematic liquid crystals, is analyzed for ferromagnetic nematics for the two cases of magnetization in or perpendicular to the shear plane. In the former case, we find that small in-plane magnetic fields are sufficient to suppress tumbling and thus that the boundary between flow alignment and tumbling can be controlled easily. In the latter case, we furthermore find a possibility of flow alignment in a regime for which one obtains tumbling for the pure nematic component. We derive the analogs of the three Miesowicz viscosities well-known from usual nematic liquid crystals, corresponding to nine different configurations. Combinations of these can be used to determine several dynamic coefficients experimentally.

I. INTRODUCTION

Many complex fluids show anisotropic and/or non-Newtonian behavior in their flow properties. A class of anisotropic complex fluids for which the flow behavior has been studied in some detail because of their wide-ranging applications are liquid crystals, in particular nematic liquid crystals [1]. Uniaxial nematics are uniaxially anisotropic liquid systems that find applications, for example, in large area displays. Clearly the flow properties of the uniaxial nematic phase are the most studied and best understood among all liquid crystalline phases [1].

In parallel, the field of magnetic liquids, i.e., suspensions of magnetic monodomain particles, has developed [2]. Various aspects of their characterization as well as of their macroscopic and microscopic properties are addressed in Refs. [3–8].

There has been considerable recent interest in a novel type of nematic phase, namely ferromagnetic nematics, showing simultaneously nematic as well as ferromagnetic order. While such a phase was predicted and investigated theoretically almost 50 years ago [9], its synthesis was reported experimentally only recently [10,11].

The ferromagnetic nematic is a room-temperature liquid multiferroic system. The only other liquid multiferroic systems known earlier are the superfluid phases of ^{3}He [12,13]. Two of them, namely ^{3}He-A and ^{3}He-A_1, are also uniaxial and show spontaneously broken orientational order as well as (anti)ferromagnetism. Besides superfluidity, both phases show rich macroscopic behavior including spin waves [14–18].

We also note that in the meantime ferromagnetic cholesteric phases have been described and characterized [19–21], thus complementing the abundant usual cholesteric phases, which break parity symmetry, because they are composed of chiral molecules: left- and right-handed helices differ from their mirror image in a nontrivial way, i.e., they cannot be brought to coincidence by mere rotations. The macroscopic behavior of ferrocholesterics has been elucidated in Ref. [22].

As for ferromagnetic nematics, most studies focused on their synthesis, their characterization, and their static properties [10,11,23]. There is also early work discussing a Landau description of phase transitions involving a ferromagnetic nematic phase [24]. A systematic investigation of their dynamic properties was initiated only quite recently [25,26]. These first two publications focused on the coupled dynamics of the two order parameters, namely the magnetization, $\mathbf{M}$, characterizing spontaneously broken rotational symmetry in spin space, and the director, $\mathbf{n}$, characteristic for systems with spontaneously broken rotational symmetry [27].

In this paper, we analyze the coupling of these two order parameters to flows generalizing simple flow situations for uniaxial nematics to ferromagnetic nematics. For the new liquid multiferroic system, we include a discussion of the analogs of effective viscosity, Miesowicz viscosities, flow alignment, as well as transient backflow [28,29] and kickback [30] effects, all familiar from usual nematics [1]. The main goal of this study is to make concrete experimentally testable predictions.

The paper is organized as follows. In Sec. II, we present the macroscopic model used throughout the present paper. In Sec. III, we discuss simple shear flow and its experimentally accessible consequences. Section IV is dedicated to a characterization of the analogs of the Miesowicz viscosities for ferromagnetic nematic liquid crystals leading to many

————
*tilen.potisk@uni-bayreuth.de

predictions. In Sec. V, we consider the analog of flow alignment and show how the transition to tumbling can be shifted by small external magnetic fields. In Sec. VI, we sketch out the effects of flow on the the dynamic behavior when an external magnetic field is switched on. In the brief last section, we conclude and give a perspective.

II. MACROSCOPIC MODEL

Throughout the present paper, we take into account the magnetization $\mathbf{M}$, the director field $\mathbf{n}$, and the velocity field $\mathbf{v}$ as macroscopic variables. For a complete set of macroscopic dynamic equations for ferronematics, we refer the reader to Refs. [31,32].

The static behavior is described by the free-energy density $f(\mathbf{M}, \mathbf{n}, \nabla \mathbf{n})$,

$$f = -\mu_0 \mathbf{M} \cdot \mathbf{H} - \tfrac{1}{2} A_1 (\mathbf{M} \cdot \mathbf{n})^2 + \tfrac{1}{2} A_2 (|\mathbf{M}| - M_0)^2 + f^F, \tag{1}$$

where μ_0 is the magnetic constant, $\mathbf{H}$ is the applied magnetic field, and $A_{1,2} > 0$ will be assumed constant. The first term represents the coupling of the magnetization and the external magnetic field. The second term describes the static coupling between the director field and the magnetization (originating from the magnetic particles). The third term describes the energy connected with the deviation of the modulus of the magnetization from M_0. The last term is the Frank elastic energy associated with director distortions [1]

$$f^F = \tfrac{1}{2} K_1 (\nabla \cdot \mathbf{n})^2 + \tfrac{1}{2} K_2 [\mathbf{n} \cdot (\nabla \times \mathbf{n})]^2 + \tfrac{1}{2} K_3 [\mathbf{n} \times (\nabla \times \mathbf{n})]^2, \tag{2}$$

with positive elastic constants for splay (K_1), twist (K_2), and bend (K_3). Throughout this paper, a one-constant approximation will be used, i.e., $K_1 = K_2 = K_3 = K$. While it is a good approximation to assume that $|\mathbf{M}| = M_0$, we will take into account small variations of $|\mathbf{M}|$ (corresponding to large values of A_2).

The total free energy is $F = \int f \, dV$ and the equilibrium condition requires $\delta F = 0$. The macroscopic dynamic equations for the magnetization, the director field, and the velocity field read [32,33]

$$\left(\frac{\partial}{\partial t} + v_j \nabla_j \right) M_i + \epsilon_{ijk} M_j \omega_k + X_i^R + X_i^D = 0, \tag{3}$$

$$\left(\frac{\partial}{\partial t} + v_j \nabla_j \right) n_i + \epsilon_{ijk} n_j \omega_k + Y_i^R + Y_i^D = 0, \tag{4}$$

$$\rho \left(\frac{\partial}{\partial t} + v_j \nabla_j \right) v_i + \nabla_j (\sigma_{ij}^R + \sigma_{ij}^D + \sigma_{ij}^{\text{th}}) - \nabla_i p = 0, \tag{5}$$

where $\omega_i = \tfrac{1}{2} \varepsilon_{ijk} \nabla_j v_k$ is the vorticity and ρ is the density. The (quasi)currents have been split into reversible ($X_i^R, Y_i^R, \sigma_{ij}^R$) and irreversible, dissipative ($X_i^D, Y_i^D, \sigma_{ij}^D$) parts. In Eq. (5), the reversible part of the stress tensor has been further split to include a thermodynamic part σ_{ij}^{th},

$$\sigma_{ij}^{\text{th}} = -B_j H_i - \tfrac{1}{2} (h_i^n n_j - h_j^n n_i) - \tfrac{1}{2} (h_i^M M_j - h_j^M M_i) + K_{kjmp} \nabla_p n_m \nabla_i n_k, \tag{6}$$

and the thermodynamic pressure

$$p = -\varepsilon + T\sigma + \mu\rho + \mathbf{g} \cdot \mathbf{v} + \mathbf{B} \cdot \mathbf{H}, \tag{7}$$

with temperature T, entropy density σ, chemical potential μ, density of linear momentum $\mathbf{g}$, and magnetic flux density $\mathbf{B}$. The reversible (dissipative) parts of the (quasi)currents have the same (opposite) behavior under time reversal as the time derivatives of the corresponding variables, i.e., Eqs. (3)–(5) are invariant under time reversal only if the dissipative (quasi) currents vanish.

The (quasi)currents are expressed as linear combinations of conjugate quantities (thermodynamic forces)

$$h_i^M \equiv \frac{\delta f}{\delta M_i} = \frac{\partial f}{\partial M_i}, \tag{8}$$

$$h_i^n \equiv \delta_{ik}^\perp \frac{\delta f}{\delta n_k} = \delta_{ik}^\perp \left(\frac{\partial f}{\partial n_k} - \partial_j \Phi_{kj} \right), \tag{9}$$

$$A_{ij} \equiv \tfrac{1}{2} (\partial_i v_j + \partial_j v_i), \tag{10}$$

with $\Phi_{kj} = \partial f / \partial (\nabla_j n_k)$ and where the transverse Kronecker delta $\delta_{ik}^\perp = \delta_{ik} - n_i n_k$ projects onto the plane perpendicular to the director due to the constraint $\mathbf{n}^2 = 1$.

In Ref. [25], only the dissipative quasicurrents X_i^D and Y_i^D were taken into account as they had a direct relevance for the explanation of the experimental results discussed there. The effects of the reversible quasicurrents X_i^R and Y_i^R were modeled in Ref. [26]. In the present paper, we also include the velocity variable in the approximation of an incompressible flow, $\nabla_i v_i = 0$.

The dissipative quasicurrents take the form [32]

$$X_i^D = b_{ij}^D h_j^M + \chi_{ji}^D h_j^n + c_{ijk}^D A_{jk}, \tag{11}$$

$$Y_i^D = \frac{1}{\gamma_1} \delta_{ik}^\perp h_k^n + \chi_{ij}^D h_j^M + \lambda_{ijk}^D A_{jk}, \tag{12}$$

$$\sigma_{ij}^D = -\nu_{ijkl}^D A_{kl} - \lambda_{kij}^D h_k^n - c_{kij}^D h_k^M, \tag{13}$$

with

$$\chi_{ij}^D = \chi_1^D \delta_{ik}^\perp M_k n_j + \chi_2^D \delta_{ij}^\perp M_k n_k, \tag{14}$$

$$b_{ij}^D = b_\parallel^D n_i n_j + b_\perp^D \delta_{ij}^\perp, \tag{15}$$

$$\begin{aligned} \nu_{ijkl}^D = {} & 2(\nu_1 + \nu_2 - 2\nu_3) n_i n_j n_k n_l \\ & + (\nu_3 - \nu_2)(n_j n_l \delta_{ik} + n_j n_k \delta_{il} + n_i n_k \delta_{jl} + n_i n_l \delta_{jk}) \\ & + (\nu_4 - \nu_2) \delta_{ij} \delta_{kl} + \nu_2 (\delta_{jl} \delta_{ik} + \delta_{il} \delta_{jk}) \\ & + (\nu_5 - \nu_4 + \nu_2)(\delta_{ij} n_k n_l + \delta_{kl} n_i n_j), \end{aligned} \tag{16}$$

$$\begin{aligned} \lambda_{ijk}^D = {} & \lambda_1^D (\delta_{iq}^\perp \epsilon_{pjq} M_p n_k + \delta_{iq}^\perp \epsilon_{pkq} M_p n_j) \\ & + \lambda_2^D (\delta_{ik}^\perp \epsilon_{pjq} M_p n_q + \delta_{ij}^\perp \epsilon_{pkq} M_p n_q) \\ & + \lambda_3^D (\epsilon_{ipk} M_j n_p + \epsilon_{ipj} M_k n_p) \\ & + \lambda_4^D M_q n_q (\epsilon_{ipk} n_j n_p + \epsilon_{ipj} n_k n_p) \\ & + \lambda_5^D \epsilon_{piq} M_p n_q n_j n_k + \lambda_6^D \epsilon_{piq} M_p n_q \delta_{jk}^\perp, \end{aligned} \tag{17}$$

$$c_{ijk}^D = c^D (\epsilon_{imk} n_m n_j + \epsilon_{imj} n_m n_k). \tag{18}$$

The tensor χ_{ij}^D describes the dissipative cross-coupling between the director and the magnetization. In Refs. [25] and [26] it was shown that it is of major importance for the dynamics and was crucial to explain the presented experiments. The viscosity tensor v_{ijkl}^D is the same as for usual nematic liquid crystals (in the Appendix, the connection with the Leslie viscosity coefficients is reviewed). The existence of the magnetization gives rise to an additional dissipative coupling of the velocity with the director, described by the tensor λ_{ijk}^D, which is not present in usual nematics. Moreover, there exists also a direct dissipative coupling of the velocity and the magnetization, described by the tensor c_{ijk}^D. Throughout the present paper, we will discard the biaxiality of the material that arises for $\mathbf{n} \nparallel \mathbf{M}$.

The reversible quasicurrents [32] are obtained by requiring that the entropy production $Y_i h_i^n + X_i h_i^M + \sigma_{ij} A_{ji}$ is zero. They are

$$X_i^R = b_{ij}^R h_j^M + \chi^R \epsilon_{ijk} n_j h_k^n - c_{ijk}^R A_{jk}, \qquad (19)$$

$$Y_i^R = (\gamma_1^{-1})_{ij}^R h_j^n + \chi^R \epsilon_{ijk} n_j h_k^M - \tfrac{1}{2} \lambda_{ijk} A_{jk}, \qquad (20)$$

$$\sigma_{ij}^R = -v_{ijkl}^R A_{kl} - \tfrac{1}{2} \lambda_{kji} h_k^n - c_{kij}^R h_k^M. \qquad (21)$$

In Eqs. (20) and (21), the reversible couplings between the velocity field on the one hand and the director field and the magnetization are described by the flow alignment tensor

$$\lambda_{ijk} = \lambda(\delta_{ij}^\perp n_k + \delta_{ik}^\perp n_j) \qquad (22)$$

and by the tensor c_{ijk}^R [32], respectively,

$$\begin{aligned} c_{ijk}^R = {} & c_1^R M_i n_j n_k + c_2^R (\delta_{ij} M_k + \delta_{ik} M_j) + c_3^R M_i \delta_{jk} \\ & + c_4^R n_i M_p n_p \delta_{jk} + c_5^R (n_i M_j n_k + n_i M_k n_j) \\ & + c_6^R n_i M_p n_p n_j n_k. \end{aligned} \qquad (23)$$

In the following, we will discard the contributions of the tensors v_{ijkl}^R, $(\gamma_1^{-1})_{ij}^R$, b_{ij}^R, and χ^R, which can be found in Ref. [32].

A. Geometry and method

In this paper, we study the situation in which a ferromagnetic nematic liquid crystal is confined between a pair of infinite parallel plates separated in the z direction by the cell thickness d. We assume that the fields are functions only of the coordinate z and time t. For solving Eqs. (3)–(5), a simple numerical method is used. We first discretize space into slices of width $\Delta z = d/(N-1)$, where N is the number of discretization points. By varying N, it is found that using $N = 50$ is already sufficient. We use a variant of the so called staggered grid, Fig. 1, to avoid possible numerical instabilities. The velocity field is defined in the middle of the slices, while the stress tensor, the director field, and the magnetization field are defined at the edges of the slices. The velocity field at these edges can be calculated simply by averaging the neighboring points,

$$v_i(j\Delta z) = 0.5\{v_i[(j-1/2)\Delta z] + v_i[(j+1/2)\Delta z]\}, \quad (24)$$

where Δz is the step size and $j \in \{0, 1, \ldots, N-1\}$ is an integer.

After discretizing space, one obtains N ordinary differential equations. For the second derivative in the bulk of the liquid-
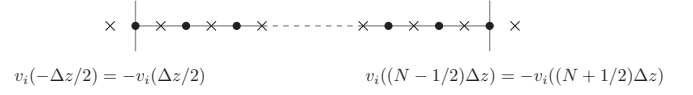
FIG. 1. A schematic representation of the staggered grid used to solve Eqs. (3)–(5). The director field, the magnetization field, and the (quasi)currents are defined on the points (black circles), while the velocity field is defined on the crosses located between the points. There are two crosses outside of the physical space, which are present in order to satisfy the boundary condition for the velocity field.

crystal cell, we used the usual central finite-difference scheme,

$$f''(z) \approx \frac{f(z + \Delta z) - 2f(z) + f(z - \Delta z)}{(\Delta z)^2} + O[(\Delta z)^2]. \qquad (25)$$

At the boundaries, we use an asymmetric finite-difference scheme for the derivatives.

Due to its simplicity, we use the Euler method for our analysis. An example for one step of the Euler method for the ith component of the director field at coordinate z is

$$n_i(t + \delta t, z) = n_i(t, z) - \delta t\, Y_i(t, z) + O(\delta t^2), \qquad (26)$$

where δt is the time step. An analogous equation holds for the magnetization field, and the equations are solved simultaneously. Since the numerical scheme for the director field is not norm-preserving, we normalize the director field after each time step: $n_i \rightarrow n_i/(n_j n_j)^{1/2}$.

The velocity field relaxes on time scales much shorter than the director field or the magnetization, and thus Eq. (5) can be simplified to

$$\nabla_j \sigma_{ij}^R + \nabla_j \sigma_{ij}^D + \nabla_j \sigma_{ij}^{\mathrm{th}} - \nabla_i p = 0. \qquad (27)$$

The equation for the pressure field can be obtained by taking the divergence of Eq. (27). The boundary conditions for the pressure are obtained by taking the inner product of Eq. (27) with the surface normals, pointing up (down) at the top (bottom) plate. The resulting pressure field is

$$p(z) = p_0 + \sigma_{zz}(z), \qquad (28)$$

where p_0 is an arbitrary constant and σ_{zz} includes all the stresses $\sigma_{zz} = \sigma_{zz}^R + \sigma_{zz}^D + \sigma_{zz}^{\mathrm{th}}$. Since p is only a function of z, it only shows up in the dynamic equation for the z component of the velocity field, where it exactly cancels out the contributions of all the stresses. The z component of the velocity field is therefore independent of time, i.e., $\partial v_z/\partial t = 0$, and is zero, $v_z = 0$, due to the boundary condition.

Given the director and the magnetization field, we solve Eq. (27) on a staggered grid for the velocity field, as shown in Fig. 1.

For the director field, we assume infinitely strong (planar) anchoring at the boundaries, $\mathbf{n} = \hat{\mathbf{e}}_x$ at $z = 0$ and $z = d$. For the velocity field, we assume the no-slip condition $\mathbf{v} = \mathbf{0}$ at $z = 0$ and $z = d$. In the case of shear experiments, $\mathbf{v} = v_{0x} \hat{\mathbf{e}}_x$ at $z = d$, where v_{0x} is the velocity of the upper plate. The lower

plate is fixed. We define the shear rate

$$\Gamma_x = \frac{v_{0x}}{d}. \tag{29}$$

B. Material parameters

Throughout this study, we will be using similar values of the static and the dynamic coefficients as determined in Ref. [25]. Therein, a ferromagnetic nematic using 5CB as a nematic solvent was studied. For the static coefficients, we used $A_1 = 130\mu_0$, $A_2 = 1000A_1$, $K = 7$ pN, $M_0 = 50$ A/m, and $d = 50$ μm and for the dynamic ones we used $\chi_2^D = 20$ (Pa s)$^{-1}$, $\chi_1^D = 0$, and $b_\perp^D = b_\parallel^D = 1.5 \times 10^5$ A m/V s^2. For the coefficients of the viscosity tensor, the rotational viscosity γ_1, and the flow alignment parameter λ, we used $\nu_1 = 0.092$ Pa s, $\nu_2 = 0.038$ Pa s, $\nu_3 = 0.045$ Pa s, $\gamma_1 = 0.081$ Pa s, and $\lambda = 1.05$; see the data for 5CB in Ref. [34]. For the remaining coefficients of ν_{ijkl}^D, we chose $\nu_4 = \nu_2$ and $\nu_5 = 0$. In the literature, one often encounters the so called Ericksen-Leslie viscosities, which are related to the set of viscosities used here (compare the Appendix for the detailed relations). For the reversible coupling c_{ijk}^R between the magnetization and the velocity field in Eqs. (19) and (21), which is the analog of the flow alignment tensor λ_{ijk} of Eqs. (20) and (21), we use the coefficient c_2^R, Eq. (23), as a representative, since it has the same structure as λ in Eq. (22). We choose the value $c_2^R = 0.55$ so that its effects on the magnetization are comparable to the effects of λ on the director field. It should be noted that for simple shear flow, the contributions of c_3^R and c_4^R are automatically zero. Furthermore, due to the approximately fixed modulus of the magnetization, the contribution of the coefficient c_1^R is negligible. The effect of c_5^R is biggest when the magnetization (director) is parallel to the velocity field and the director (magnetization) is perpendicular to the velocity field and within the shear plane, which is perpendicular to the vorticity. Lastly, the effect of c_6^R is biggest when the magnetization is either parallel or perpendicular to the velocity field and the director is at 45° with respect to the magnetization while both fields are in the shear plane.

III. SIMPLE SHEAR

A classical approach to study the rheology of simple and complex fluids is the investigation of a simple shear flow. Here we will focus on the changes compared to the case of uniaxial nematics by the application of a magnetic field perpendicular to the plates of a shear cell.

In this section, we discard the dissipative couplings of the director and the magnetization to the velocity field, i.e., the tensors λ_{ijk}^D and c_{ijk}^D of Eqs. (17) and (18) are set to zero. From the form of the tensor λ_{ijk}^D (c_{ijk}^D) one can see that there is, in general, a nonzero coupling between the out-of-shear plane component of the director (magnetization) field with the part of the director (magnetization) molecular field h_i^n (h_i^M), which is within the shear plane. Since we have set these tensors to zero, the velocity points along the x axis everywhere with the director and the magnetization being within the shear plane, which is also confirmed numerically.

In Fig. 2 we present the solutions of v_x/v_{0x}, n_z, and M_z/M_0 as functions of z. A magnetic field $\mathbf{H} = H\hat{\mathbf{e}}_z$ of
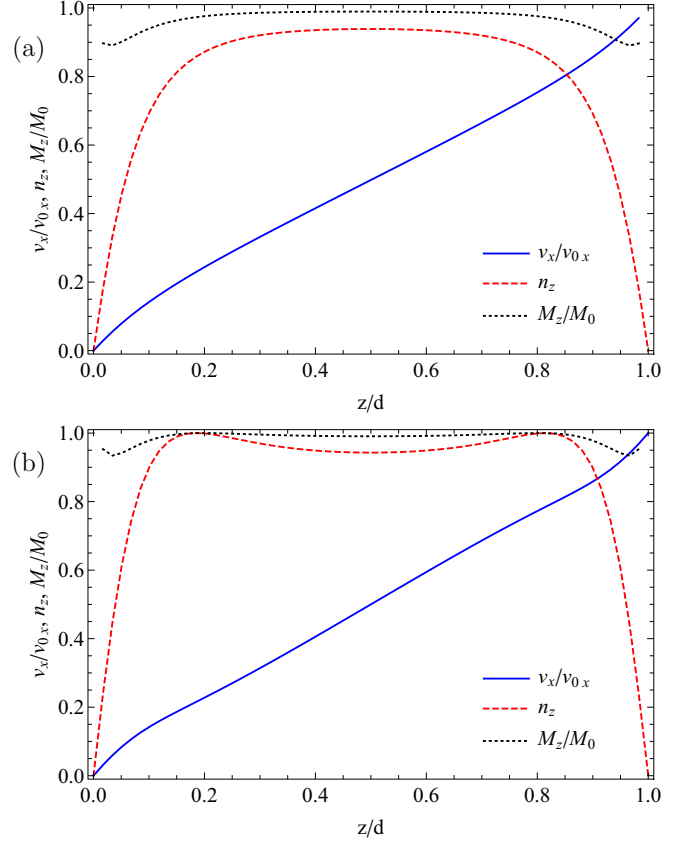
FIG. 2. Profiles of v_x/v_{0x}, M_z/M_0, and n_z at a shear rate $\Gamma_x = 1$ s^{-1} with (a) $\mu_0 H = 10$ mT and (b) $\mu_0 H = -10$ mT.

$H = 10$ mT [Fig. 2(a)] and $H = -10$ mT [Fig. 2(b)] was applied perpendicularly to the plates, and a shear rate of $\Gamma_x = 1$ s^{-1} was imposed. We observe that for the negative magnetic field, the director in the middle of the cell rotates by an angle of more than $\pi/2$. This is due to the fact that the shear forces, which are described by the tensor λ_{ijk}, change direction at a certain orientation of the director. This orientation is determined by the parameter λ. Secondly, it is more favorable for the director to rotate further, since the coupling energy (A_1) gets lower.

The dependence of the x component of the velocity field on the magnetic field at a shear rate of 1 s^{-1} is shown in Fig. 3. One can see, as expected, that the velocity profile is not linear, and a boundary layer of order 10% of the cell thickness is visible using $\Gamma_x = 1$ s^{-1} and magnetic fields of order 1 mT. The thickness of the boundary layer of the velocity field can be connected with the deformation of the director field, where the boundary layer is determined by the competition of the forces related to the static coupling A_1 and the Frank elastic forces.

The quantity that is normally measured is the effective viscosity of the sheared sample, i.e., the shear force per unit area σ_{xz} exerted by the fluid on the glass plate divided by the shear rate Γ_x. In the present system, one must, however, take into account that the Maxwell stress $-B_j H_i$, unlike all the other contributions to the stress tensor, does not end at the boundary of the fluid as the magnetic flux continues into the glass plate. Consequently, the Maxwell stress does not contribute to the
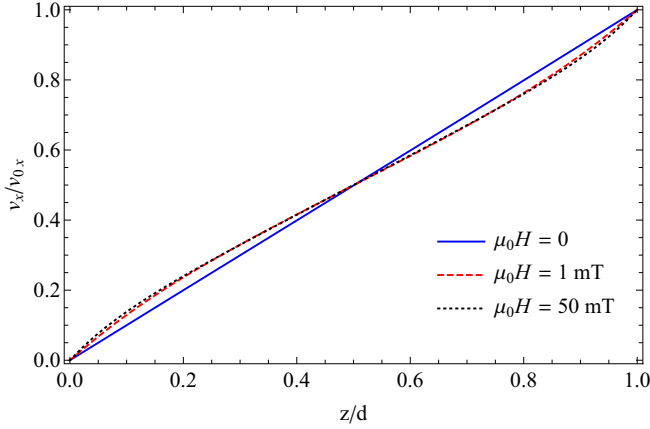
FIG. 3. The normalized x component of the velocity field v_x/v_{0x} for different values of the applied magnetic field at a shear rate $\Gamma_x = 1 \, \text{s}^{-1}$.

force on the glass plate. This is best seen by calculating the force as the integral of σ_{xz} over a pair of planes tightly enclosing the $z = d$ interface. In the resulting difference of shear stresses across the interface, $[\sigma_{xz}]$, all contributions to $\sigma_{xz}(z = d)$ are recovered as usual, except the term $-B_j H_i$ of Eq. (6), which cancels out. The effective viscosity is thus

$$\nu^{\text{eff}} = \frac{[\sigma_{xz}]}{\Gamma_x}. \tag{30}$$

In Fig. 4, the effective viscosity is plotted as a function of the magnetic field for two values of the shear rate Γ_x, which are equal in magnitude but opposite in sign.

Most strikingly, a rather large increase in the effective viscosity by about a factor of 2 can be achieved by applying a rather small magnetic field of about 20 mT; see Fig. 4(a). The reason the effective viscosity increases at very low fields is due to the response of the magnetization and the director field in an external magnetic field, which was studied in detail in Ref. [26]. There it was shown analytically that the configuration of the system, i.e., the director and the magnetization field, saturates quickly above a characteristic magnetic field determined by the static coupling, $\mu_0 H \sim A_1 M_0$, which for the parameters used here is approximately 10 mT. The viscosity increases as **n** and **M** rotate toward getting perpendicular to the velocity field and lying within the shear plane. This opens the door to an easily accessible viscosity control for a nematic fluid system by using small magnetic fields.

In addition, we see that—just as the absolute value of the vertical component of the director—also the effective viscosity is invariant with respect to the transformation $\Gamma_x \to -\Gamma_x$, $\mu_0 H \to -\mu_0 H$.

As we increase the magnetic field, we see that the effective viscosity first saturates at fairly low magnetic fields of order 30 mT, Fig. 4(a). A similar effect has been observed in experiments using 8CB [35]. There, a rather complex shear geometry was used, therefore the experimental results cannot be mapped in a straightforward manner onto the results presented here.

In should be noted that we take into account also the diamagnetic contribution, $-\frac{1}{2}\mu_0 \chi_a (\mathbf{n} \cdot \mathbf{H})^2$, with a diamagnetic anisotropy, $\chi_a = 5 \times 10^{-6}$. For small magnetic fields, Fig. 4(a),
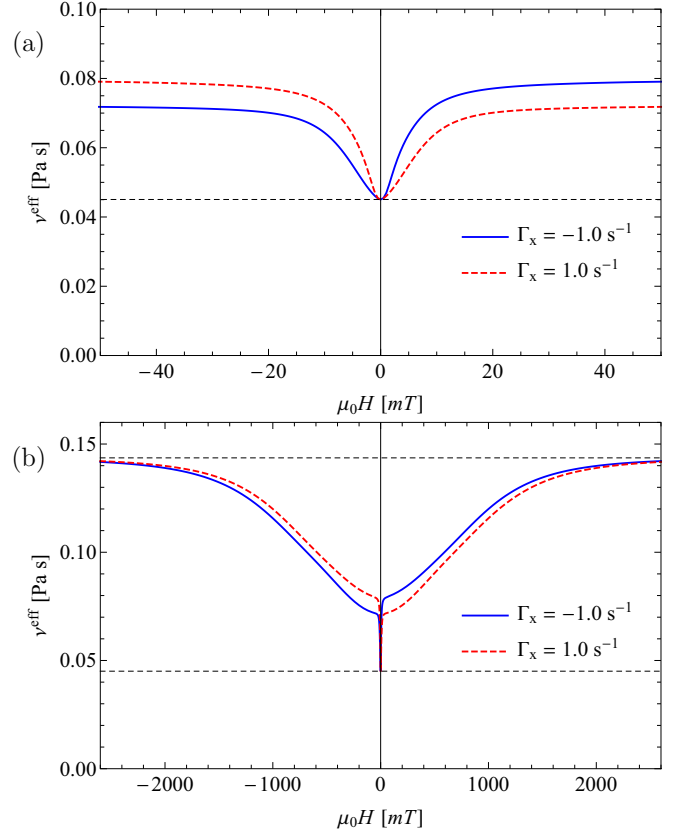
FIG. 4. The behavior of the effective viscosity for (a) small and (b) large values of the applied magnetic field at oppositely equal shear rates. The dashed lines represent two of the Miesowicz viscosities (η_{xx} and η_{zz}), defined in Sec. IV.

the effects of this term are very small, which is verified by comparing the numerical results with $\chi_a = 0$. On the other hand, if we increase the magnetic field further, the viscosity starts to increase again; see Fig. 4(b). This is due to the diamagnetic anisotropy, which tries to align the director along the external magnetic field. The viscosity finally saturates at fields of order 1 T, where the director field along with the magnetization field point approximately along the applied magnetic field. In the limit of large magnetic fields, the director and the magnetization both point along z and, therefore, the effective viscosity converges to one of the Miesowicz viscosities, η_{zz} [dashed line in Fig. 4(b)], defined and calculated in Sec. IV. In the absence of the magnetic field, the director and the magnetization point approximately along the x axis, which means the effective viscosity approaches the value of another Miesowicz viscosity, η_{xx} [dashed line in Fig. 4(a)]. The behavior at larger magnetic fields is a prediction, which can be experimentally tested.

In Fig. 4 one also observes that the effective viscosity strongly increases when one increases the magnetic field from the intermediate saturation region at 50 mT to a large magnetic field of order of 1 T. A possible explanation for such a dramatic increase can be deduced from Fig. 5, where we present the profiles of the fields v_x/v_{0x}, M_z/M_0, and n_z at these two magnetic fields. For the lower magnetic field, Fig. 5(a), the boundary layer ξ^l of n_z is of order of 10% of the cell thickness,
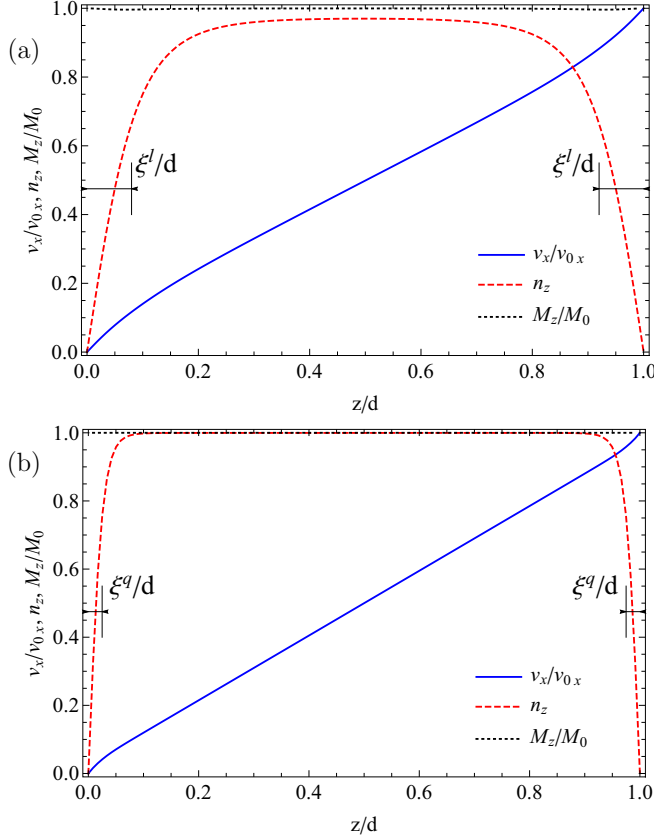
FIG. 5. Profiles of v_x/v_{0x}, M_z/M_0, and n_z at a shear rate $\Gamma_x = 1\,\mathrm{s}^{-1}$ with (a) $\mu_0 H = 50\,\mathrm{mT}$ and (b) $\mu_0 H = 1\,\mathrm{T}$. The boundary layers for (a) the lower magnetic field, ξ^l, and (b) the higher magnetic field, ξ^q, can be estimated from Eqs. (31) and (32), respectively.

which can be estimated from the parameter q of Eq. (39), discussed in the next subsection:

$$\frac{\xi^l}{d} \sim \sqrt{\frac{K}{A_1 M_0^2 d^2}} \approx 0.1. \tag{31}$$

In the large magnetic-field limit, the diamagnetic energy term is dominant. Equating the typical Frank elastic energy with the typical diamagnetic energy gives us a boundary layer ξ^q of 2% of the cell thickness:

$$\frac{\xi^q}{d} \sim \sqrt{\frac{K}{\mu_0 \chi_a H^2 d^2}} \approx 0.02. \tag{32}$$

Smaller boundary layers for the director field mean stronger elastic forces close to the boundaries. These forces increase the shear stress and therefore also the effective viscosity.

It should be noted that a crossover from a ferromagnetic response linear in H, for small fields, to a regime quadratic in H, for large fields, has also been observed in uniaxial magnetic gels [36], a class of soft matter systems that also shows rich macroscopic behavior [37].

A. Small shear rate behavior

For small shear rates, n_z increases linearly as we increase the shear rate. This can be shown analytically by first assuming that

the velocity profile is linear, i.e., $\mathbf{v} = \Gamma_x z \hat{\mathbf{e}}_x$. We furthermore discard the dissipative cross-couplings between the velocity field and the director or the magnetization, described by the tensors λ_{ijk}^D and c_{ijk}^D, Eqs. (17) and (18). Consequently, there are no terms in the dynamic equations (4) and (3) that couple the thermodynamic forces to the currents in the y direction. The fields thus stay within the shear (xz) plane,

$$\mathbf{n} = \cos\theta \hat{\mathbf{e}}_x + \sin\theta \hat{\mathbf{e}}_z,$$
$$\mathbf{M}/M_0 = \cos\psi \hat{\mathbf{e}}_x + \sin\psi \hat{\mathbf{e}}_z. \tag{33}$$

The dynamic equations for the angles θ and ψ then read

$$\frac{\partial\theta}{\partial t} = -\frac{1}{2}\Gamma_x[1 - \lambda\cos(2\theta)] + \frac{K}{\gamma_1}\frac{\partial^2\theta}{\partial z^2}$$
$$- \frac{A_1 M_0^2}{8}\left(\chi_1^D + \chi_2^D\right)\sin[4(\psi - \theta)]$$
$$+ \mu_0 H M_0\left[\chi_2^D\cos^2(\psi - \theta) - \chi_1^D\sin^2(\psi - \theta)\right]\cos\psi$$
$$+ \frac{A_1 M_0^2}{4}\left(\frac{2}{\gamma_1} + \chi_1^D - \chi_2^D\right)\sin[2(\psi - \theta)], \tag{34}$$

$$\frac{\partial\psi}{\partial t} = -\frac{1}{2}\Gamma_x\left[1 - 2c_2^R\cos(2\psi)\right] + \frac{b_\perp^D}{M_0^2}\mu_0 H M_0\cos\psi$$
$$+ \frac{1}{2}\left\{\left(\chi_1^D + \chi_2^D\right)\cos[2(\psi - \theta)] - \chi_1^D + \chi_2^D\right\}K\frac{\partial^2\theta}{\partial z^2}$$
$$+ \frac{A_1 M_0^2}{8}\left(\chi_1^D + \chi_2^D\right)\sin[4(\psi - \theta)]$$
$$- \frac{A_1 M_0^2}{4}\left(\frac{2b_\perp^D}{M_0^2} + \chi_1^D - \chi_2^D\right)\sin[2(\psi - \theta)]. \tag{35}$$

In the small-magnetic-field limit, we can use the small-angle approximation ($\theta, \psi \ll 1$). Setting the time derivatives $\partial\theta/\partial t$ and $\partial\psi/\partial t$ to zero, the solution for the angle θ reads

$$\theta(z) = \frac{\Gamma_x}{4K\left(\frac{b_\perp^D}{\gamma_1 M_0^2} - \left(\chi_2^D\right)^2\right)}\left[(\lambda - 1)\left(\chi_2^D - \frac{b_\perp^D}{M_0^2}\right)\right.$$
$$\left. - \left(2c_2^R - 1\right)\left(\frac{1}{\gamma_1} - \chi_2^D\right)\right]z(z - d)$$
$$- \frac{\mu_0 H M_0}{2K}z(z - d), \tag{36}$$

from which one can see that for small magnetic fields and shear rates, n_z is linear in both of them. In the limit $\Gamma_x \to 0$, one obtains a solution in agreement with the one in Ref. [26]. It is interesting to note that for small shear rates and in the absence of the magnetic field, the angle can decrease as one increases the shear rate, provided that the following inequality is satisfied:

$$2c_2^R > 1 + (\lambda - 1)\frac{\chi_2^D - \frac{b_\perp^D}{M_0^2}}{\frac{1}{\gamma_1} - \chi_2^D}. \tag{37}$$

It is rather realistic that this inequality is satisfied using known and/or extracted values of the involved parameters.

In the large magnetic-field limit, the director and the magnetization point approximately along the z axis. The solution for the angles θ^+ (θ^-) for positive (negative) magnetic
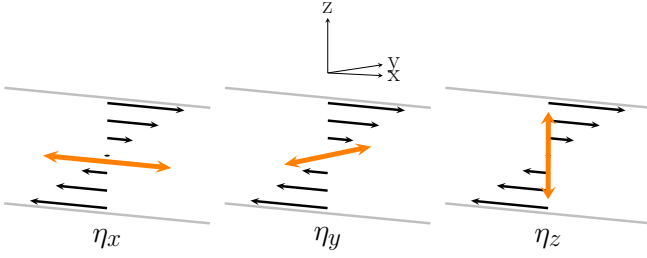
FIG. 6. Miesowicz viscosities in a usual nematic liquid crystal. The director field is indicated in orange.

fields is

$$\theta^{\pm}(z) = \pm\frac{\pi}{2} - C\Gamma_x \mp \left(\frac{\pi}{2} \mp C\Gamma_x\right)\frac{\cosh\left[q(z-d/2)\right]}{\cosh\left(qd/2\right)},$$ (38)

where

$$q^2 = q_0^2 \frac{\mu_0|H|M_0}{A_1 M_0^2 + \mu_0|H|M_0},$$ (39)

with $q_0 = \sqrt{A_1 M_0^2 / K}$, and C is a constant determined by the dynamic and the static parameters:

$$C = \frac{\gamma_1(1+\lambda)b_\perp^D + (1-d_2)M_0^2}{2\mu_0|H|M_0\left(b_\perp^D - \left[\chi_2^D\right]^2\gamma_1 M_0^2\right)}$$
$$+ \frac{\gamma_1(1+\lambda)b_\perp^D - \left(1+2c_2^R\right)\chi_2^D\gamma_1 M_0^2}{2A_1 M_0^2\left(b_\perp^D - \left[\chi_2^D\right]^2\gamma_1 M_0^2\right)}$$ (40)

with the abbreviation $d_2 = 2c_2^R(\chi_2^D\gamma_1 - 1) + \chi_2^D\gamma_1(2+\lambda)$. We point out that Eq. (38) correctly predicts the fact that the director can rotate by more than $\pi/2$ in the middle of the cell, as is observed in Fig. 2.

IV. MIESOWICZ VISCOSITIES

There exists a number of different ways one can measure viscosities of a nematic liquid crystal. The earliest technique and a particularly useful one is the concept of Miesowicz viscosities, where one fixes by an external magnetic or electric field the director and exposes the system to a shear flow [38,39]. Depending on the relative orientation of the director with respect to the velocity field or the shear plane, Fig. 6, there exist, for sufficiently high external fields, three limiting cases of the measured viscosities: η_x when $\mathbf{n} = \hat{\mathbf{e}}_x$, η_y when $\mathbf{n} = \hat{\mathbf{e}}_y$, and η_z when $\mathbf{n} = \hat{\mathbf{e}}_z$. The shear flow is applied in the xz plane. These Miesowicz viscosities are

$$\eta_x = \nu_3 + \frac{\gamma_1}{4}(\lambda - 1)^2,$$ (41)

$$\eta_y = \nu_2,$$ (42)

$$\eta_z = \nu_3 + \frac{\gamma_1}{4}(\lambda + 1)^2.$$ (43)

Below, we derive analogous viscosities for the ferromagnetic nematic liquid crystal. Since we have the additional variable of magnetization, not only are the expressions for the viscosities different but there are also more possible
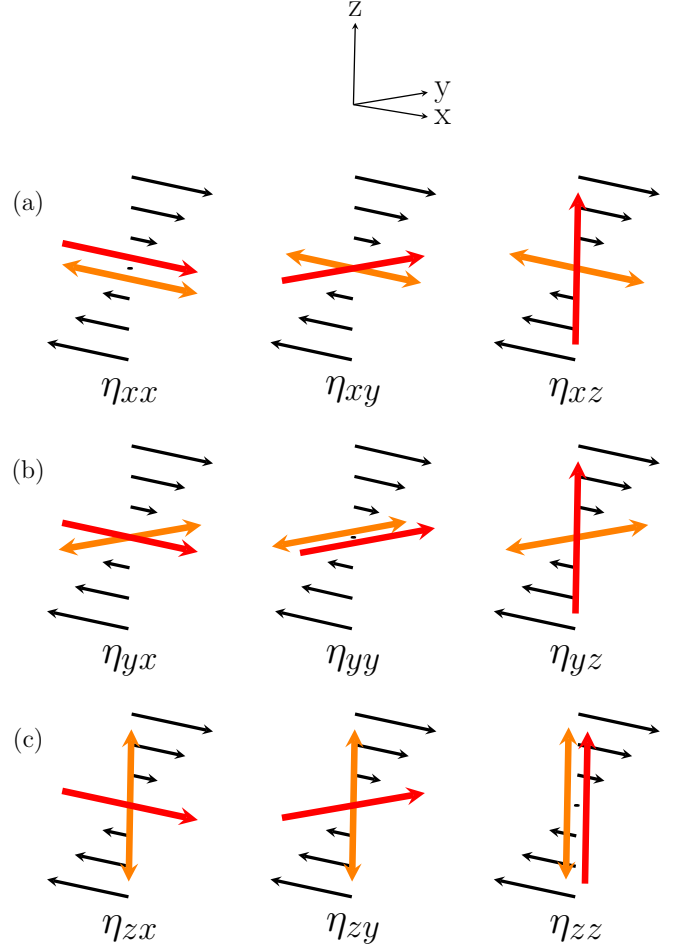
FIG. 7. Analogs of the Miesowicz viscosities in a ferromagnetic nematic liquid crystal, when the director (orange) is along the (a) x, (b) y, and (c) z axis. The magnetization is shown in red.

combinations. We will denote the analogous viscosities by $\eta_{\alpha\beta}$, where $\alpha, \beta \in \{x, y, z\}$ represent the fixed directions of the director and the magnetization, respectively.

A simple shear flow $v_x(z) = \Gamma_x z$, $v_y(z) = 0$, $v_z(z) = 0$ is imposed. The resulting nine independent possible configurations of the magnetization and the director are shown in Fig. 7.

To simplify the expressions, we have set, besides the tensors ν_{ijkl}^R, $(\gamma_1^{-1})_{ij}^R$, b_{ij}^R, and χ^R, also the tensors λ_{ijk}^D and χ_1^D to zero, which is the same as in Sec. III, but here we keep c_{ijk}^D, Eq. (18). To derive the Miesowicz viscosities, one first sets the quasicurrents X_i and Y_i to zero. From this one obtains the thermodynamic forces h_i^n and h_i^M, Eqs. (9) and (8), as a function of the shear rate Γ_x. Finally, one uses the thermodynamic forces in the expression for the xz component of the total stress tensor σ_{xz}.

When the director is along the x axis, Fig. 7(a), the three independent viscosities are

$$\eta_{xx} = \nu_3 + \frac{1}{4}\left(1 - \frac{(\chi_2^D)^2 M_0^2\gamma_1}{b_\perp^D}\right)^{-1}\left[\gamma_1(1-\lambda)^2 - 4(c^D)^2\right.$$
$$\left. + \frac{M_0^2}{b_\perp^D}(1-2c_2^R)\left[1 - 2c_2^R - 2\chi_2^D\gamma_1(1-\lambda)\right]\right],$$ (44)

$$\eta_{xy} = \nu_3 + \frac{\gamma_1}{4}(1-\lambda)^2 - \frac{(c^D)^2}{b_\perp^D}, \tag{45}$$

$$\eta_{xz} = \nu_3 + \frac{\gamma_1}{4}(1-\lambda)^2 - \frac{(c^D)^2}{b_\perp^D} + \frac{M_0^2\left(1 + 2c_2^R + 2c_5^R\right)^2}{4b_\parallel^D}. \tag{46}$$

When the director is along the y axis, Fig. 7(b), the three independent viscosities are

$$\eta_{yx} = \nu_2 + \frac{M_0^2\left(1 - 2c_2^R\right)^2}{4b_\perp^D}, \tag{47}$$

$$\eta_{yy} = \nu_2, \tag{48}$$

$$\eta_{yz} = \nu_2 + \frac{M_0^2\left(1 + 2c_2^R\right)^2}{4b_\perp^D}. \tag{49}$$

One can see that in the case in which the director and the magnetization are both perpendicular to the shear plane, the viscosity is $\eta_{yy} = \eta_y = \nu_2$, as in ordinary nematic liquid crystals.

When the director is along the z axis, Fig. 7(c), the viscosities are similar as in the case when the director is along the x axis. One can get the viscosities η_{zi} from η_{xi} by the transformation $\lambda \to -\lambda$, $c_2^R \to -c_2^R$, $c_5^R \to -c_5^R$, and $x \leftrightarrow z$. This can be explained by the fact that the contributions of λ, c_2^R, and c_5^R in the quasicurrents change sign as one rotates the director or the magnetization by $90°$ within the shear plane. We thus have

$$\eta_{zx} = \nu_3 + \frac{\gamma_1}{4}(1+\lambda)^2 - \frac{(c^D)^2}{b_\perp^D} + \frac{M_0^2\left(1 - 2c_2^R - 2c_5^R\right)^2}{4b_\parallel^D}, \tag{50}$$

$$\eta_{zy} = \nu_3 + \frac{\gamma_1}{4}(1+\lambda)^2 - \frac{(c^D)^2}{b_\perp^D}, \tag{51}$$

$$\eta_{zz} = \nu_3 + \frac{1}{4}\left(1 - \frac{\left(\chi_2^D\right)^2 M_0^2 \gamma_1}{b_\perp^D}\right)^{-1} \times \left[\gamma_1(1+\lambda)^2 - 4(c^D)^2\right.$$
$$\left. + \frac{M_0^2}{b_\perp^D}\left(1 + 2c_2^R\right)\left[1 + 2c_2^R - 2\chi_2^D\gamma_1(1+\lambda)\right]\right]. \tag{52}$$

We observe that the viscosities reduce to Miesowicz viscosities, Eqs. (41)–(43), in the limit $c^D \to 0$ and $M_0 \to 0$.

In Refs. [25,26], the value of the dissipative cross-coupling coefficient χ_2^D was shown to be large and thus it should strongly affect the values of the Miesowicz viscosities η_{xx} and η_{zz} as compared with the nematic analogs η_x and η_y.

One notices that the Miesowicz viscosities only contain the coefficients c_2^R and c_5^R of c_{ijk}^R. As discussed in Sec. III, for simple shear the coefficients c_3^R and c_4^R do not contribute. The coefficient c_1^R is irrelevant due to the fixed modulus M_0. The contributions of c_6^R are zero in the chosen configurations, which is due to either the fixed modulus or the perpendicular orientations of the director and the magnetization.

We emphasize that important relations between the nine Miesowicz viscosities exist, e.g.,

$$\eta_{yz} - \eta_{yx} = \frac{M_0^2 c_2^R}{b_\perp^D}, \tag{53}$$

$$\eta_{zz} - \eta_{xx} = \frac{b_\perp^D \gamma_1 \lambda - \left[2c_2^R\left(\chi_2^D\gamma_1 - 1\right) + \chi_2^D\gamma_1\lambda\right]M_0^2}{b_\perp^D - \left(\chi_2^D\right)^2 M_0^2 \gamma_1}, \tag{54}$$

$$\eta_{zx} - \eta_{xz} = \gamma_1\lambda - \frac{M_0^2\left(c_2^R + c_5^R\right)}{b_\parallel^D}, \tag{55}$$

which can be used to determine certain combinations of dynamic coefficients experimentally.

V. FLOW ALIGNMENT

In this section, we study the flow alignment in a ferromagnetic nematic. For usual uniaxial nematics, this is a well-known phenomenon, where under the influence of a simple shear flow the director is tilted by a finite angle with respect to the velocity field. In the case of uniaxial nematics, this angle is determined by the flow alignment parameter λ, which is a reversible transport coefficient and not associated with any dissipation. For biaxial nematics and for mixtures of uniaxial nematics, various aspects of flow alignment have also been addressed [40–44]. In ferromagnetic nematic liquid crystals, we have to take into account also the dynamics of the magnetization. This means that in simple shear flow, generally, the director and the magnetization are not parallel.

We investigate the case in which the shear flow is imposed with the external magnetic field pointing along the x axis, $\mathbf{H} = H\hat{\mathbf{e}}_x$, as opposed to the case in Sec. III in which the magnetic field points in z direction. This direction of the magnetic field is chosen to ensure that the director and the magnetization field are in the presence of a magnetic field homogeneous across the cell. The homogeneous response makes it convenient to analyze the ferromagnetic nematic flow alignment as a function of the applied magnetic field. The contribution of the Frank elastic term, Eq. (2), can thus be discarded. Generally, there exists a boundary layer with thickness

$$\xi^v \sim \sqrt{\frac{K}{\gamma_1 \Gamma_x}}, \tag{56}$$

which decreases with increasing shear rate. This boundary layer is defined by a competition between the viscous forces and the elastic forces. In the limit $\xi^v/d \ll 1$, the velocity profile is linear, $\mathbf{v} = \Gamma_x z\hat{\mathbf{e}}_x$. For the parameters used in this study, this limit can be achieved using shear rates $\Gamma_x \gg 0.03$ s^{-1}. We remind the reader that two different boundary layers, corresponding to the deformation of the director field in a magnetic field, are defined in Sec. III, Eqs. (31) and (32). Since we discard the elastic forces, these boundary layers are zero.

As is done in Sec. III, we again discard the dissipative cross-couplings between the velocity field and the director or the magnetization, Eqs. (17) and (18). In this case, the director and the magnetization both stay in the shear (xz) plane and can be described by Eq. (33), as discussed in Sec. III.

The dynamic equations for the angles θ and ψ are then similar to those presented in Sec. III, Eqs. (34) and (35), with the difference being in the term describing the magnetic field

and in the absence of elastic forces:

$$
\frac{\partial \theta}{\partial t} = -\frac{1}{2} \Gamma_x [1 - \lambda \cos(2\theta)] - \frac{A_1 M_0^2}{8} \chi_2^D \sin[4(\psi - \theta)]
$$
$$
- \chi_2^D \mu_0 H M_0 \cos^2(\psi - \theta) \sin(\psi)
$$
$$
+ \frac{A_1 M_0^2}{4} \left(\frac{2}{\gamma_1} - \chi_2^D \right) \sin[2(\psi - \theta)], \tag{57}
$$

$$
\frac{\partial \psi}{\partial t} = -\frac{1}{2} \Gamma_x \left[1 - 2 c_2^R \cos(2\psi) \right] + \frac{A_1 M_0^2}{8} \chi_2^D \sin[4(\psi - \theta)]
$$
$$
- \frac{b_\perp^D}{M_0^2} \mu_0 H M_0 \sin(\psi)
$$
$$
- \frac{A_1 M_0^2}{4} \left(\frac{2 b_\perp^D}{M_0^2} - \chi_2^D \right) \sin[2(\psi - \theta)], \tag{58}
$$

where, for simplicity, c_2^R is taken as a representative of c_{ijk}^R, and χ_2^D is set to zero. A stationary solution exists if $\partial\theta/\partial t = 0$ and $\partial\psi/\partial t = 0$.

In the limit of large shear rates ($\Gamma_x \gg \frac{A_1 M_0^2}{\gamma_1}$) and in zero magnetic field, we obtain

$$
\cos(2\theta) = \frac{1}{\lambda}, \tag{59}
$$

$$
\cos(2\psi) = \frac{1}{2 c_2^R}. \tag{60}
$$

The solutions of Eqs. (59) and (60) are $\theta = \pm\frac{1}{2}\arccos(1/\lambda)$ and $\psi = \pm\frac{1}{2}\arccos(1/2c_2^R)$. A linear stability analysis of Eqs. (57) and (58) has been done, where the angles are perturbed from their stationary values θ_0 and ψ_0, i.e., $\theta = \theta_0 + \delta\theta$ and $\psi = \psi_0 + \delta\psi$. We find that for positive (negative) shear rates, the positive (negative) angle is the stable solution.

In the large magnetic-field limit, $\frac{b_\perp^D}{M_0^2}\mu_0 H M_0 \gg \frac{A_1 M_0^2}{\gamma_1}$, while still assuming that the effects of the diamagnetic anisotropy are negligible, stationary solutions $\psi^\pm$ for the magnetization angle are

$$
\sin\psi^\pm = -\frac{\Gamma_x^H}{\Gamma_x} \pm \sqrt{\left(\frac{\Gamma_x^H}{\Gamma_x} \right)^2 + \frac{2 c_2^R - 1}{4 c_2^R}}, \tag{61}
$$

where

$$
\Gamma_x^H = \frac{b_\perp^D}{4 c_2^R M_0^2} \mu_0 H M_0 \tag{62}
$$

is the characteristic "magnetic" shear rate determined by the magnetic field.

It has not been possible to make the analytical solution for the angle θ tractable. We thus only present the asymptotic behavior of this angle and for completeness also the asymptotic behavior of the angle ψ. From Eq. (61) one can see that in the limit $\Gamma_x / \Gamma_x^H \ll 1$ one finds, to first order,

$$
\psi^+ = \frac{2 c_2^R - 1}{8 c_2^R} \frac{\Gamma_x}{\Gamma_x^H}, \tag{63}
$$

$$
\tan\theta^+ = \sqrt{ \frac{b_\perp^D(\lambda - 1) - (2 c_2^R - 1)\chi_2^D M_0^2}{b_\perp^D(1 + \lambda)} }
$$
$$
- \frac{(2 c_2^R - 1)^2 \chi_2^D M_0^2}{8 b_\perp^D c_2^R(1 + \lambda)} \frac{\Gamma_x}{\Gamma_x^H}, \tag{64}
$$
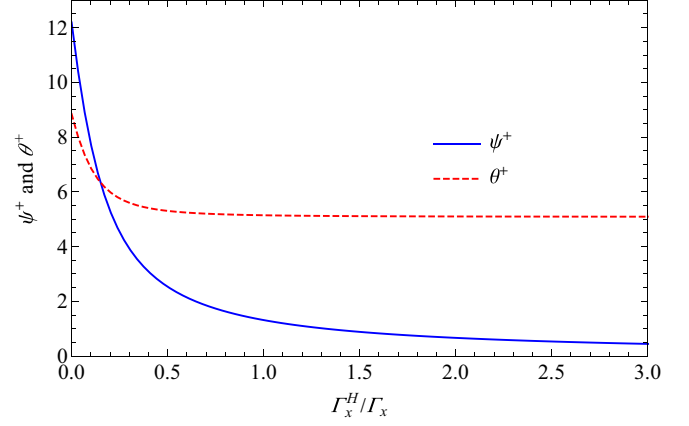
FIG. 8. The theoretical dependence of the magnetization ψ^+ (blue curve) and director θ^+ (red dashed curve) angles in degrees as functions of the dimensionless ratio of the characteristic magnetic shear rate [Eq. (62)] and the applied shear rate, Γ_x^H / Γ_x.

while ψ^- does not exist and $\tan\theta^+$ is calculated by inserting the solution for the angle ψ^+ from Eq. (61) into Eq. (57). It is tractable to perform a linear stability analysis of the solution Eq. (58) analytically, finding the stability condition

$$
\pm c_2^R \Gamma_x \sqrt{ \left(\frac{\Gamma_x^H}{\Gamma_x} \right)^2 + \frac{2 c_2^R - 1}{4 c_2^R} } > 0, \tag{65}
$$

where the sign $\pm$ corresponds to the solutions $\psi^\pm$. From Eq. (65) we see that the solution ψ^+ (ψ^-) is stable if the product $c_2^R \Gamma_x$ is positive (negative).

In Fig. 8 we present the numerical solutions of Eqs. (57) and (58) for the angles ψ^+ and θ^+ as functions of Γ_x^H / Γ_x. As predicted in Eqs. (63) and (64), we see that the angle ψ^+ decreases to zero, while the angle θ^+ saturates at a finite value as the field is increased.

In the absence of the magnetic field and in the large shear rate limit, the stationary solution exists if $|\lambda| \geqslant 1$ and $|c_2^R| \geqslant \frac{1}{2}$. In usual nematic liquid crystals, if $|\lambda| < 1$ holds, the system shows a tumbling behavior. In such a system flow alignment can be recovered if a sufficiently large electric field is applied; see Refs. [45,46]. In our system, this could be achieved with the use of low magnetic fields.

To check this possibility, one must first ensure the existence of the solutions Eq. (61). Secondly, we are only interested in the stable solutions, i.e., Eq. (65) must hold. We find that the required magnetic field depends on four different ranges of the c_2^R values:

$$
c_2^R < 0, \quad \pm\Gamma_x < 0, \quad \frac{\Gamma_x^H}{\Gamma_x} > \mp\frac{1 + 2 c_2^R}{8 c_2^R}, \tag{66}
$$

$$
0 < c_2^R < \frac{1}{6}, \quad \pm\Gamma_x > 0, \quad \frac{\Gamma_x^H}{\Gamma_x} > \pm\frac{1 + 2 c_2^R}{8 c_2^R}, \tag{67}
$$

$$
\frac{1}{6} < c_2^R < \frac{1}{2}, \quad \pm\Gamma_x > 0, \quad \frac{\Gamma_x^H}{\Gamma_x} > \pm\sqrt{\frac{1 - 2 c_2^R}{4 c_2^R}}, \tag{68}
$$

$$
c_2^R > \frac{1}{2}, \quad \pm\Gamma_x > 0, \quad \frac{\Gamma_x^H}{\Gamma_x} > \mp\frac{1 + 2 c_2^R}{8 c_2^R}, \tag{69}
$$

where the signs $\pm$ correspond to the two solutions Eq. (61).

Another stationary solution of the dynamic equations is found when the director is in the shear plane, while the magnetization is perpendicular to this plane,

$$\mathbf{n} = \cos\theta\,\hat{\mathbf{e}}_x + \sin\theta\,\hat{\mathbf{e}}_z, \tag{70}$$

$$\mathbf{M} = M_0\hat{\mathbf{e}}_y. \tag{71}$$

In this case, we do not discard any dynamic coefficients. The solution for the angle θ is

$$\tan(\theta) = \frac{\lambda_{\text{eff}}^D M_0}{\lambda + 1} \pm \sqrt{\left(\frac{\lambda_{\text{eff}}^D M_0}{\lambda + 1}\right)^2 + \frac{\lambda - 1}{\lambda + 1}}, \tag{72}$$

where $\lambda_{\text{eff}}^D = 2\lambda_1^D + 2\lambda_2^D - \lambda_5^D + \lambda_6^D$. A solution exists if the term under the square root is positive, leading to the condition

$$\lambda^2 \geqslant 1 - \left(\lambda_{\text{eff}}^D M_0\right)^2. \tag{73}$$

This means that one can observe flow alignment in a ferromagnetic nematic, even if the pure nematic solvent shows tumbling behavior.

We investigated the stability of the solution Eq. (72) numerically. We find that it is stable in the absence of a magnetic field if the static coupling (A_1) between the director and the magnetization is negative, because in that case $\mathbf{n} \perp \mathbf{M}$ is the equilibrium orientation. For a positive A_1, even the slightest perturbation in the magnetization field drives the director toward it, since it is favorable for them to be parallel rather than perpendicular. The solution Eq. (72) can nevertheless be made stable for ferromagnetic nematics with positive A_1, provided one uses a large magnetic field in the y direction and the diamagnetic anisotropy χ_a is negative. This is to ensure that the director stays within the shear plane and the magnetization is perpendicular to it.

The case discussed above, in which the magnetization is perpendicular to the shear plane and the director is in the shear plane at an angle θ with respect to the velocity field, most closely resembles one of the possible stationary solutions of a biaxial nematic liquid crystal exposed to a shear flow; see Ref. [43]. In the latter system, the angle of one of the preferred directions with respect to the velocity field is given by the reversible coupling of the corresponding variable to the velocity field. In contrast, in ferromagnetic nematic liquid crystals this angle is determined by both the reversible and the dissipative coupling of the director to the velocity field.

VI. SWITCH-ON DYNAMICS

In this section, we study the reorientation of the director and the magnetization in an external magnetic field applied perpendicularly to the glass plates, $\mathbf{H} = H\hat{\mathbf{e}}_z$. We are particularly interested in the influence of flow on this transient dynamics. Unlike in the previous sections, flow is not externally imposed, but is generated by the reorientation dynamics itself, i.e., by backflow. Throughout this section, the dissipative cross-coupling between the magnetization and the velocity c_{ijk}^D, Eq. (18), is set to zero.

As a first step, we take into account only the reversible cross-coupling λ_{ijk} between the director and the velocity, Eqs. (20)–(22), while the analog cross-coupling c_{ijk}^R between
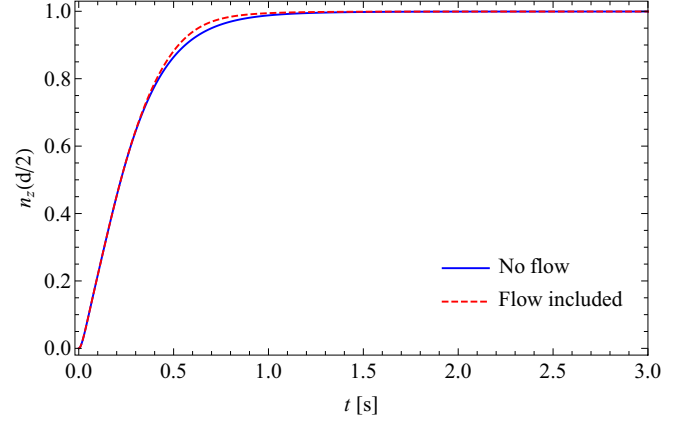
FIG. 9. The theoretical time dependence of n_z in the middle of the cell, for the cases with and without inclusion of flow, $\mu_0 H = 5$ mT. In the former case, only the flow alignment tensor λ_{ijk} and the viscous tensor ν_{ijkl}^D are taken into account in the dynamics.

the magnetization and the velocity, Eqs. (19), (21), and (23), is set to zero. Figure 9 shows the time dependence of n_z in the midplane of the cell ($z = \frac{d}{2}$). A comparison is made between cases with and without inclusion of flow. We find that the influence of the reversible director–flow coupling is small and makes the transient dynamics a little faster; see Fig. 9. This has also been readily encountered in usual nematic liquid crystals [28,29]. We find furthermore that a strong dissipative cross-coupling between the director and the magnetization makes these backflow effects even less visible. To isolate them, we have set the tensor χ_{ij}^D, Eq. (14), to zero.

When the term c_2^R of the cross-coupling c_{ijk}^R, Eq. (23), is included in addition to λ_{ijk}, the backflow effects are similar, i.e., the dynamics is only slightly faster. This is not surprising, since the tensor λ_{ijk} and the term c_2^R have a similar form.

On the other hand, we find that the dissipative cross-coupling between the director and the velocity λ_{ijk}^D, Eq. (17), which is absent in usual nematics, can have a somewhat larger influence, Fig. 10. In our numerical calculations, we used the coefficient λ_3^D as the representative of the tensor λ_{ijk}^D, i.e., $\lambda_{ijk}^D = \lambda_3^D(\epsilon_{ipk}M_j n_p + \epsilon_{ipj}M_k n_p)$.

The reason for this choice is that at $t = 0$, when both $\mathbf{n}$ and $\mathbf{M}$ are parallel and within the xz plane, λ_3^D provides a nonzero contribution to the director quasicurrent component Y_y. The same is true for the coefficients λ_1^D and λ_4^D, while the initial contributions of λ_2^D, λ_5^D, and λ_6^D are zero. It should be noted that, due to the additional dissipative cross-coupling λ_{ijk}^D, the velocity field has a general orientation somewhere in the xy plane and hence $\mathbf{n}$ and $\mathbf{M}$ wander out of the xz plane, Fig. 10(b). This is in contrast to the case in Sec. III, where the velocity points along the x direction throughout the cell, and $\mathbf{n}$ and $\mathbf{M}$ stay in the shear plane.

The v_x and v_y profiles at four different moments are presented in Fig. 11 in terms of the Ericksen number, defined as the ratio of viscous and elastic forces on the director,

$$\text{Er}_i = \frac{\gamma_1 v_i d}{K}, \tag{74}$$
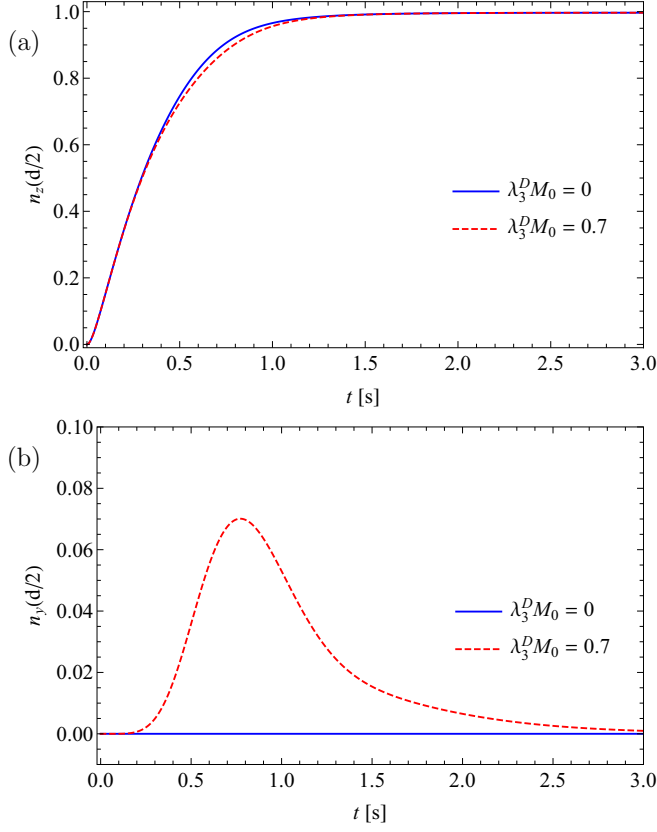
FIG. 10. The theoretical time dependence of the (a) z and (b) y component of the director field at $\mu_0 H = 5$ mT for two different values of λ_3^D.

with i corresponding to either the x or y velocity component. For the chosen value of λ_3^D, the maximum values in both directions are comparable, $\mathrm{Er}_x \sim \mathrm{Er}_y \sim 2$.

It should be noted that the values of the dissipative cross-coupling coefficients are fundamentally restricted by the positivity of the entropy production. In our case (zero χ_1^D, χ_2^D,
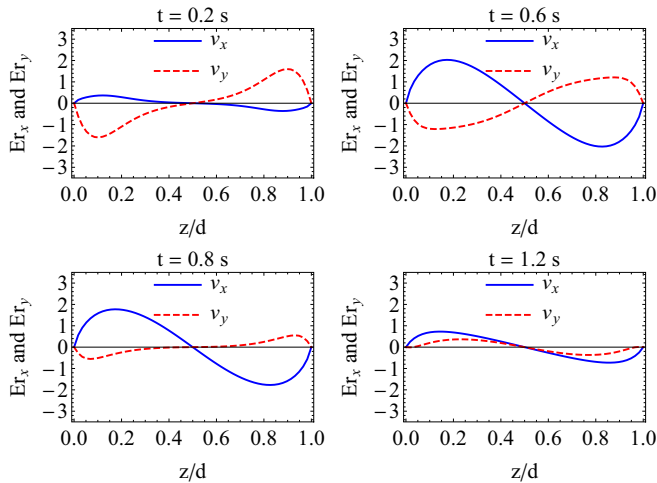
FIG. 11. Backflow profiles in terms of the Ericksen numbers Er_x and Er_y, Eq. (74), at four moments of time; $\mu_0 H = 5$ mT, $\lambda_3^D M_0 = 0.7$.
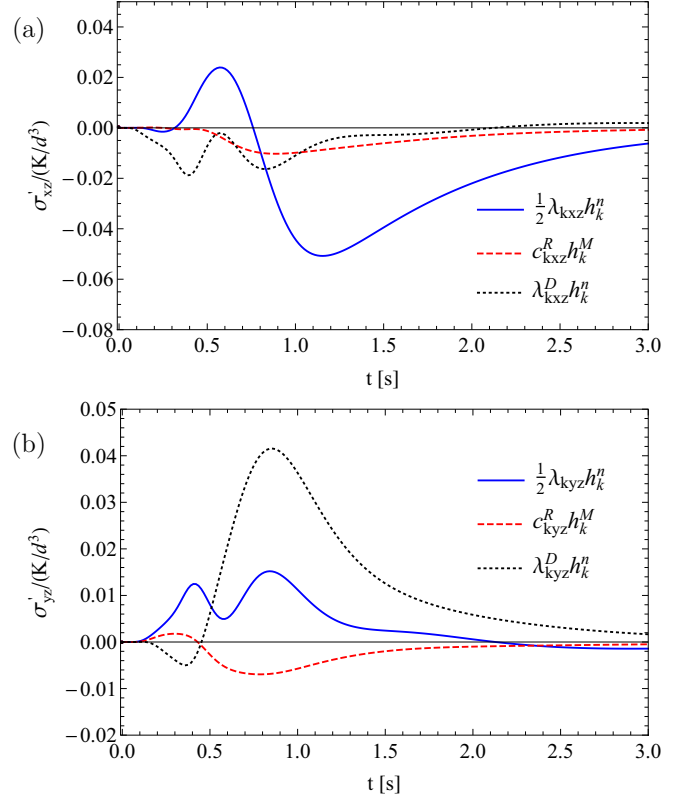
FIG. 12. The x and y components of the stress tensor divergence (a) $\sigma'_{xz} = \partial \sigma_{xz}/\partial z$ and (b) $\sigma'_{yz} = \partial \sigma_{yz}/\partial z$, at $z = d/2$, in units of characteristic divergence of the elastic stress K/d^3 for each of the three different backflow-driving stress tensor contributions explained in the text.

and c^D), the restriction is

$$\left| \lambda_3^D M_0 \right| \lesssim \sqrt{\frac{\nu_3}{\gamma_1}} \sim 0.75, \tag{75}$$

where ν_3 is chosen as the representative of the tensor ν_{ijkl}.

We are interested in the importance of specific contributions to components σ_{xz} and σ_{yz} of the stress tensor. These are the usual nematic backflow-driving stress $\frac{1}{2}\lambda_{kij}h_k^n$, the analogous stress corresponding to the dynamics of the magnetization, $c_{kij}^R h_k^n$, and the stress from the dissipative director–velocity cross-coupling, $\lambda_{kij}^D h_k^n$. The divergence of these stresses has nonzero x and y components that are individually presented in Fig. 12.

We first analyze the σ_{xz} component, Fig. 12(a). The contributions of $c_{kxz}^R h_k^n$ and $\lambda_{kxz}^D h_k^n$ are smaller than those of $\frac{1}{2}\lambda_{kxz}h_k^n$. This can be explained by two facts. First, at any moment the director field is much more deformed than the magnetization field, which means that the thermodynamic force h_i^n, Eq. (9), will have a much bigger impact on the divergence of the stress than the thermodynamic force h_i^M, Eq. (8). This automatically explains that the backflow from the director field $\frac{1}{2}\lambda_{kxz}h_k^n$ is bigger than that from the magnetization $c_{kxz}^R h_k^n$. Secondly, the contribution $\lambda_{kxz}^D h_k^n$ is proportional to $\lambda_3^D n_y M_z h_z^n$. Since n_y is never large [Fig. 10(b)], neither is the contribution of $\lambda_{kxz}^D h_k^n$.

The situation is different for the σ_{yz} component. Figure 12(b) reveals that the contribution of $\lambda_{kyz}^D h_k^n$ is the biggest. This can be explained by writing its leading term as $\lambda_3^D n_x M_z h_z^n$, which does not contain n_y. The leading terms of the backflow contributions, $\frac{1}{2}\lambda_{kyz} h_k^n$ and $c_{kyz}^R h_k^n$, are smaller in comparison, since they are always proportional to either n_y and M_y, or to h_y^n and h_y^M.

Next, we are interested in the magnitude of the flow generated when a magnetic field is applied perpendicularly to the plates in one case and a voltage difference is applied across the plates in the other case. The magnitude of the flow is measured using the Ericksen number Er_x, Eq. (74), which we have calculated using the maximum magnitude of the velocity across the cell. We find that $\mathrm{Er}_x \sim 1$ can be achieved using either a rather small magnetic field of 3 mT or a voltage difference of 2.5 V.

We conclude this section by pointing out that there are no effects of flow on the initial dynamics, at least up to first order in time. This can be shown by expanding the currents in Eqs. (3)–(5). Since the initial thermodynamic forces h_i^n and h_i^M are homogeneous, the generated stress σ_{ij} in Eq. (5) is also homogeneous. Its divergence, which generates flow, is thus absent initially. Consequently, Eqs. (3) and (5) are initially also unaffected by flow. It is the dissipative cross-coupling coefficient χ_2^D between the director and the magnetization that gives a linear time dependence of n_z, as was shown in Ref. [25] and discussed in Ref. [26].

VII. CONCLUSIONS AND PERSPECTIVE

In this paper, we have analyzed the consequences of some simple flows on various configurations of ferromagnetic nematic liquid crystals. These flows include simple shear flow, the determination of transport coefficients in the spirit of Miesowicz, and the analog of flow alignment for ferromagnetic nematics.

For the case of simple shear, we find that the effective viscosity can be increased by a factor of about 2 for rather small magnetic fields of about 20 mT. This effect can be tuned continuously in magnitude simply by varying the external magnetic field. For the determination of transport coefficients, we analyze the analog of the three Miesowicz configurations well-known from usual uniaxial nematics. Since one can fix the director and the direction of the spontaneous magnetization by external electric and magnetic fields, it is now possible to analyze nine independent different geometries. We find that these various geometries can be used to determine experimentally combinations of coefficients including dissipative and reversible terms characteristic of a system with a director, a magnetization, and a velocity field as macroscopic variables.

For the analog of flow alignment in usual uniaxial nematics, we find simple stationary solutions without an external magnetic field involving an orientation of both the director and the magnetization for the case in which both of these variables are in the shear plane in the limit of sufficiently large shear. In addition, we show that a small external magnetic field can shift the boundary between tumbling and flow alignment. For the case in which the magnetization $\mathbf{M_0}$ is perpendicular to the shear plane and the director $\mathbf{n}$ is lying in the shear plane, we find for a range of parameters that a ferromagnetic nematic can reveal flow alignment, although the nematic solvent by itself shows tumbling.

As a perspective, we point out that we are aware of only one experimental publication investigating the effect of flow on ferromagnetic nematics, namely the effects of shear flow in a rather complicated geometry [35]. These experimental results are compatible with our theoretical results in the sense that they show qualitatively similar behavior as a function of an external magnetic field and a viscosity enhancement effect of comparable magnitude. In a next step, it is highly desirable to compare experimental and theoretical results quantitatively for a simple and well-controlled geometry. There appear to be no experimental results available so far for the question of flow alignment and the evaluation of transport coefficients, parallel to the Miesowicz concept, for ferromagnetic nematics. Clearly, any experimental results in these two directions will stimulate refinement of the modeling of this exciting first liquid multiferroic system at room temperatures.

APPENDIX: LESLIE COEFFICIENTS

In the Ericksen-Leslie formulation of nematodynamics, a different set of coefficients is used. The Leslie coefficients are defined [1] by the symmetrized stress tensor

$$\sigma_{ij}^{\mathrm{EL}} = \alpha_1 n_i n_j n_k n_p A_{kp} + (\alpha_2 + \alpha_3)(n_i N_j + n_j N_i) + \alpha_4 A_{ij} + (\alpha_5 + \alpha_6)(n_i n_k A_{jk} + n_j n_k A_{ik}), \quad (A1)$$

and the molecular field

$$h_i^{\mathrm{EL}} = \gamma_1 N_i + \gamma_2 n_j A_{ij}, \quad (A2)$$

with $\gamma_2 = \alpha_3 + \alpha_2$ being a reversible transport parameter, not a viscosity. Here, the superscript EL denotes Ericksen-Leslie, $N_i = \partial n_i / \partial t - \omega_{ij} n_j$ is the corotational time derivative of the director—or rather its dissipative quasicurrent, $-Y_i^D$ [Eq. (4)], and $\omega_{ij} = \frac{1}{2}(\partial v_i / \partial x_j - \partial v_j / \partial x_i)$ is the vorticity tensor.

The set of Leslie coefficients is related to the coefficients of the tensor ν_{ijkl}^D [33]:

$$\alpha_1 = 2(\nu_1 + \nu_2 - 2\nu_3) - \gamma_1 \lambda^2, \quad (A3)$$

$$\alpha_2 + \alpha_3 = -\gamma_1 \lambda, \quad (A4)$$

$$\alpha_4 = 2\nu_2, \quad (A5)$$

$$\alpha_5 + \alpha_6 = 4(\nu_3 - \nu_2) + \gamma_1 \lambda^2. \quad (A6)$$

The flow alignment parameter $\lambda = -\gamma_2/\gamma_1$ is expressed as the ratio of reversible transport parameter γ_2 and the rotational viscosity γ_1.

[1] P. G. de Gennes and J. Prost, *The Physics of Liquid Crystals* (Clarendon Press, Oxford, 1995).

[2] R. E. Rosensweig, *Ferrohydrodynamics* (Cambridge University Press, Cambridge, 1985).

[3] S. Odenbach, J. Phys.: Condens. Matter **16**, R1135 (2004).

[4] H.-W. Müller and M. Liu, Phys. Rev. E **64**, 061405 (2001).

[5] B. Huke and M. Lücke, Rep. Prog. Phys. **67**, 1731 (2004).

[6] P. Ilg, E. Coquelle, and S. Hess, J. Phys.: Condens. Matter **18**, S2757 (2006).

[7] S. Mahle, P. Ilg, and M. Liu, Phys. Rev. E **77**, 016305 (2008).

[8] S. D. Peroukidis and S. H. L. Klapp, Phys. Rev. E **92**, 010501 (2015).

[9] F. Brochard and P. G. de Gennes, J. Phys. (France) **31**, 691 (1970).

[10] A. Mertelj, D. Lisjak, M. Drofenik, and M. Čopič, Nature (London) **504**, 237 (2013).

[11] A. Mertelj and D. Lisjak, Liq. Cryst. Rev. **5**, 1 (2017).

[12] A. J. Leggett, Rev. Mod. Phys. **47**, 331 (1975).

[13] J. C. Wheatley, Rev. Mod. Phys. **47**, 415 (1975).

[14] R. Graham, Phys. Rev. Lett. **33**, 1431 (1974).

[15] R. Graham and H. Pleiner, Phys. Rev. Lett. **34**, 792 (1975).

[16] M. Liu, Phys. Rev. Lett. **43**, 1740 (1979).

[17] H. Brand, M. Dorfle, and R. Graham, Ann. Phys. (NY) **119**, 434 (1979).

[18] H. Brand and H. Pleiner, J. Phys. (France) **43**, 369 (1982).

[19] Q. Zhang, P. J. Ackerman, Q. Liu, and I. I. Smalyukh, Phys. Rev. Lett. **115**, 097802 (2015).

[20] P. J. Ackerman and I. I. Smalyukh, Nat. Mater. **16**, 426 (2017).

[21] P. Medle Rupnik, D. Lisjak, M. Čopič, S. Čopar, and A. Mertelj, Sci. Adv. **3**, e1701336 (2017).

[22] H. R. Brand, A. Fink, and H. Pleiner, Eur. Phys. J. E **38**, 65 (2015).

[23] A. Mertelj, N. Osterman, D. Lisjak, and M. Čopič, Soft Matter **10**, 9065 (2014).

[24] H. Pleiner, E. Jarkova, H.-W. Müller, and H. R. Brand, Magnetohydrodynamics **37**, 254 (2001).

[25] T. Potisk, D. Svenšek, H. R. Brand, H. Pleiner, D. Lisjak, N. Osterman, and A. Mertelj, Phys. Rev. Lett. **119**, 097802 (2017).

[26] T. Potisk, A. Mertelj, N. Sebastián, N. Osterman, D. Lisjak, H. R. Brand, H. Pleiner, and D. Svenšek, Phys. Rev. E **97**, 012701 (2018).

[27] D. Forster, *Hydrodynamic Fluctuations, Broken Symmetries and Correlation Functions* (Benjamin, Reading, MA, 1995).

[28] D. Svenšek and S. Žumer, Liq. Cryst. **28**, 1389 (2001).

[29] D. Svenšek and S. Žumer, Continuum Mech. Thermodyn. **14**, 231 (2002).

[30] J. Turk and D. Svenšek, Phys. Rev. E **89**, 032508 (2014).

[31] E. Jarkova, H. Pleiner, H.-W. Müller, A. Fink, and H. R. Brand, Eur. Phys. J. E **5**, 583 (2001).

[32] E. Jarkova, H. Pleiner, H.-W. Müller, and H. R. Brand, J. Chem. Phys. **118**, 2422 (2003).

[33] H. Pleiner and H. R. Brand, in *Pattern Formation in Liquid Crystals*, edited by A. Buka and L. Kramer (Springer, New York, 1996).

[34] L. M. Blinov and V. G. Chigrinov, *Electrooptic Effects in Liquid Crystal Materials* (Springer, New York, 1996).

[35] R. Sahoo, M. V. Rasna, D. Lisjak, A. Mertelj, and S. Dahra, Appl. Phys. Lett. **106**, 161905 (2015).

[36] D. Collin, G. K. Auernhammer, O. Gavat, P. Martinoty, and H. R. Brand, Macromol. Rapid Commun. **24**, 737 (2003).

[37] S. Bohlius, H. R. Brand, and H. Pleiner, Phys. Rev. E **70**, 061411 (2004).

[38] M. Miesowicz, Nature (London) **136**, 261 (1935).

[39] M. Miesowicz, Nature (London) **158**, 27 (1946).

[40] H. Brand and H. Pleiner, Phys. Rev. A **24**, 2777 (1981).

[41] M. Liu, Phys. Rev. A **24**, 2720 (1981).

[42] A. Saupe, J. Chem. Phys. **75**, 5118 (1981).

[43] H. Brand and H. Pleiner, J. Phys. **43**, 853 (1982).

[44] H. Pleiner and H. R. Brand, J. Phys. **46**, 615 (1985).

[45] K. Skarp and T. Carlsson, Mol. Cryst. Liq. Cryst. **49**, 75 (1978).

[46] T. Carlsson and K. Skarp, Mol. Cryst. Liq. Cryst. **78**, 157 (1981).